



HAL
open science

Assessment of the mechanical properties of soft tissues phantoms using impact analysis

Arthur Bouffandeau, Anne-Sophie Poudrel, Chloé Brossier, Giuseppe Rosi, Vu-Hieu Nguyen, Charles-Henri Flouzat-Lachaniette, Jean-Paul Meningaud, Guillaume Haiat

► **To cite this version:**

Arthur Bouffandeau, Anne-Sophie Poudrel, Chloé Brossier, Giuseppe Rosi, Vu-Hieu Nguyen, et al.. Assessment of the mechanical properties of soft tissues phantoms using impact analysis. *Skin Research and Technology*, In press. hal-04769785

HAL Id: hal-04769785

<https://hal.science/hal-04769785v1>

Submitted on 12 Nov 2024

HAL is a multi-disciplinary open access archive for the deposit and dissemination of scientific research documents, whether they are published or not. The documents may come from teaching and research institutions in France or abroad, or from public or private research centers.

L'archive ouverte pluridisciplinaire **HAL**, est destinée au dépôt et à la diffusion de documents scientifiques de niveau recherche, publiés ou non, émanant des établissements d'enseignement et de recherche français ou étrangers, des laboratoires publics ou privés.

Assessment of the mechanical properties of soft tissues phantoms using impact analysis

Arthur Bouffandeau¹, Anne-Sophie Poudrel¹, Chloé Brossier¹, Giuseppe Rosi², Vu-Hieu Nguyen², Charles-Henri Flouzat-Lachaniette^{3,4}, Jean-Paul Meningaud^{4,5}, and Guillaume Haiat¹

¹**CNRS, University Paris East Creteil, University Gustave Eiffel, UMR 8208, MSME, F-94010 Créteil, France.**

²**University Paris East Creteil, University Gustave Eiffel, CNRS, UMR 8208, MSME, F-94010 Créteil, France.**

³**Orthopaedic and Trauma Surgery Department, Hospital Henri Mondor AP-HP, University Paris East, F-94000 Créteil, France**

⁴**INSERM U955, IMRB University Paris East, F-94000 Créteil, France .**

⁵**Aesthetic and Maxillofacial Surgery Department, Hospital Henri Mondor AP-HP, F-94000 Créteil, France.**

Corresponding author:

Guillaume HAÏAT

Laboratoire de Modélisation et de Simulation Multi Echelle, UMR CNRS 8208,

61 avenue du Général de Gaulle,

94010 Créteil, France

tel : (33) 1 45 17 14 41

fax : (33) 1 45 17 14 33

e-mail : guillaume.haiat@cnrs.fr

Abstract

Background - The skin physiopathological conditions have a strong influence on its biomechanical properties. However, it remains difficult to accurately assess the surface stiffness of soft tissues, which would be useful to help clinicians for diagnosis and/or therapeutic monitoring purposes.

Materials and Methods – The aim of this study was to evaluate the performances of an impact-based analysis method (IBAM) and to compare them with those of an existing digital palpation device, the MyotonPro®. The IBAM functional principle is based on the indicator Δt derived from the signal corresponding to the temporal variation of the force obtained during the impact of an instrumented hammer equipped with a force sensor on a cylindrical punch in contact with agar-based phantoms mimicking soft tissues. Various phantom geometries, stiffnesses and structures (homogeneous and bilayer) were used to estimate the performances of both methods.

Results – During the measurements, the IBAM is shown to be sensitive to a volume of interest that can be approximated by a sphere of diameter around twice that of the punch. The sensitivity of the IBAM to changes of Young's modulus is comprised between 2.2 and 5.4 kPa according to the range considered, which is similar to the sensitivity of dynamic mechanical analysis (DMA), and significantly better compared to MyotonPro. The axial (respectively lateral) resolution is 2 (respectively 5) times lower with IBAM than with MyotonPro.

Conclusion - The IBAM is a simple, cheap, reproducible, quantitative and non-invasive method. The present study paves the way for the development of a decision-support system for the measurement of the skin biomechanical properties.

Accepted by Skin Research and Technology

25

Keywords: soft tissues; impact analysis; elastography; mechanical properties; instrumentation

1. Introduction

Despite its empirical nature, palpation has long been used to inspect tissues biomechanical properties and identify potential pathologies such as for instance cancer or fibrosis^{1,2}, which induce modifications of the mechanical properties of soft tissues³. In dermatology and plastic surgery, the skin biomechanical property is a marker of interest in scleroderma, keloid scars, various cancerous tumors or Ehlers-Danlos syndromes^{4,5}. Additionally, the cosmetics industry is interested in the characterization of the skin firmness to assess the effectiveness of their products^{6,7} and to propose a product in a customer-specific manner. A simple, reliable, objective and non-invasive method of soft tissues biomechanical characterization is likely to be used as a decision-support system in various fields of medicine and cosmetics, which could motivate the development of a personalized medicine approach allowing improved diagnosis, monitoring and evaluation of therapeutic response^{7,8}.

Elastography has emerged in the 1990s and is based on the estimation of the elastic moduli of soft tissues⁹. Transient elastography has become a reference tool in clinical practice to retrieve the soft tissues elastic modulus, like for example in the diagnosis of hepatic fibrosis^{10,11}. However, due to its complexity and cost, and to the fact that its performances are limited when it comes to analyse the surface of soft tissues, the use of elastography for the evaluation of skin properties remains limited. For this reason, new relatively low-cost, easy-to-use devices have emerged. For example, the Cutometer® exploits the principle of suction to exert a deformation on the skin and thus to characterize the skin superficial layers^{6,7,12}. However, the method presents certain limitations in terms of reproducibility and interpretation in relation to the viscoelastic parameters of the skin^{6,7}. In the same context, MyotonPro® is a handheld digital palpation device for research use only, which records biomechanical parameters of soft tissues based on their response to a mechanical impulse^{13,14}. This device has been used in the context of physiotherapy, neurology, dermatology or sports medicine.

Interestingly, a method based on impact analysis has recently been developed and tested with agar-based soft tissues phantoms¹⁵. This method derives from a technique initially developed in the framework of orthopedic surgery to assess the stability of cementless hip arthroplasty, acetabular cup¹⁶⁻¹⁸ and femoral stem¹⁹⁻²¹, based on impact analysis. A hammer instrumented with a force sensor was used to record the variation of the force as a function of time during an impact realized on the bone-implant system. The force signals were analysed and a time indicator was shown to be related to the implant stability. The technique was then

applied to osteotomy procedures^{22,23} and, more specifically, to rhinoplasty^{24,25}. The impact-based analysis method (IBAM) tested with agar-based soft tissues phantoms¹⁵ showed that a time indicator obtained from the impact signals was sensitive to the agar mass concentration. However, it was not possible to determine the mechanical properties of the samples and the set-up suffered from reproducibility issues. Moreover, the IBAM could not be compared quantitatively with other existing techniques in its ability to predict the sample Young's modulus.

The aim of this article is to evaluate the performances (in terms of lateral and axial resolution as well as of sensitivity) of the IBAM to retrieve the soft tissues biomechanical properties and to compare them with those of MyotonPro® device. To do so, agar-based soft tissue mimicking phantoms have been considered²⁶⁻²⁹ with various agar mass concentrations^{30,31}. The elastic moduli of the samples have been measured using a custom vibration-based set-up. The performances of both devices in terms of i) axial and lateral resolutions and ii) sensitivity of changes of phantoms Young's modulus was compared by considering homogeneous and bilayer phantoms.

2. Materials and methods

2.1. Samples preparation

In order to mimic the mechanical properties of soft tissue, several phantoms made of an agar hydrogel were fabricated following Manickam *et al.*²⁶ with different stiffness values depending on the agar mass concentration comprised between 1% to 5%. To prepare the hydrogel for a mass concentration of agar t_{ag} , a solution containing a volume V_w of distilled water and a mass m_{ag} of agar powder were mixed in a beaker with:

$$m_{ag} = \frac{t_{ag} \times V_w \times \rho_w}{1 - t_{ag}} \quad (1)$$

where ρ_w is the density of the distilled water. The mixture was then heated using a heating magnetic stirrer. At the boiling point, heating was stopped and the mixture was cooled while maintaining stirring. When the temperature reached 60°C, the hydrogel was poured into the mold and placed in the refrigerator for 20 minutes to finalize the gelation process. Finally, the sample was removed from the mold and stored overnight (minimum 12 hours) in distilled water in the refrigerator. Before each manipulation, the sample was returned to room temperature for

at least one hour. To avoid dehydration and hence alteration of the phantom's properties, the phantom was removed from the water just before the measurements and repositioned in the water no more than 10 minutes after its removal³².

Depending on the experiment, the samples could be homogeneous or bilayer. For example, in the case of the preparation of a bilayer phantom with 2% and 5% agar mass concentration, a first 2% agar hydrogel was prepared according to the method described above and poured into the mold until half-full. During the gelation process in the refrigerator, the second 5% agar hydrogel was prepared with the same method and poured into the rest of the mold.

2.2 Impact-based analysis method (IBAM)

The experimental set-up for the mechanical characterization method by impact analysis was described in Poudrel *et al.*¹⁵ and is shown in Fig. 1. Briefly, it consists of a 5-gram hammer, equipped with a force transducer (type 8204, Brüel and Kjær (B&K), Naerum, Denmark) impacting a 35 mm long and 4 mm diameter cylindrical aluminum punch in contact with the upper surface of the phantom to be characterized. As shown in Fig. 1, the system was integrated into a support that holds the agar sample and guides the punch vertically during the measurements. Note that this positioning system has been improved in terms of phantom positioning, punch guidance and impact properties compared to Poudrel *et al.*¹⁵.

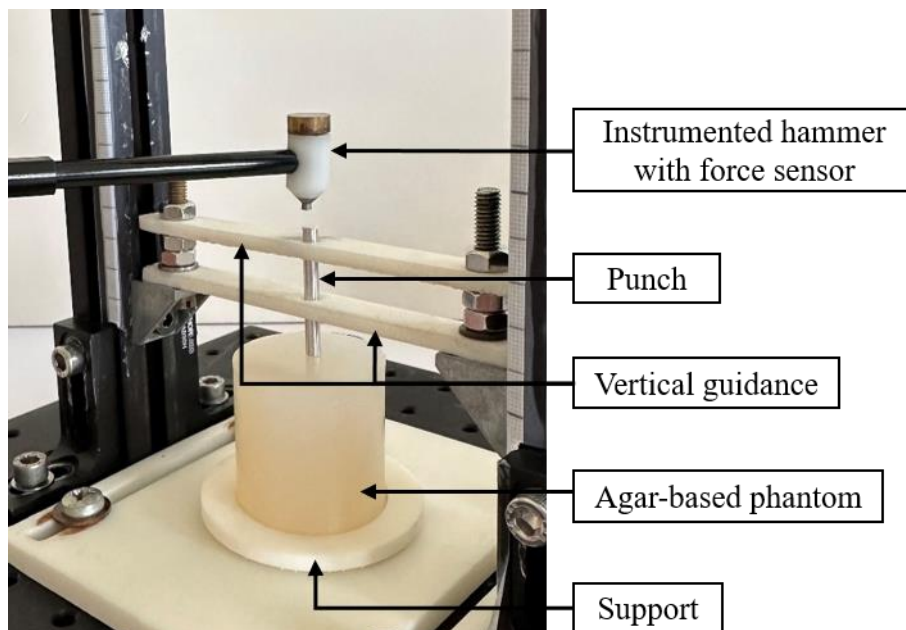


Figure 1: Experimental set-up of the impact-based analysis (IBAM) method. During a measurement, the instrumented hammer impacts the punch, which is vertically guided. The lower part of the punch is in contact with the agar-based phantom held by the support.

The variation of the force as a function of time obtained during the impact of the instrumented hammer on the punch was measured as the output data of the force transducer using LabVIEW software (National Instruments, Austin, TX, USA) and a data acquisition module with a sampling frequency of 102.4 kHz (NI 9234, National Instruments, Austin, TX, USA). A typical signal is shown in Fig. 2. The first peak corresponds to the initial impact of the hammer on the punch, denoted by $t_{i,1}$, and the following peaks are related to the rebounds of the punch between the hammer and the phantom^{15,22}. The maximum value of the first peak is referred to as impact force IF in what follows. Similarly, the time of the first rebound, corresponding to the second peak, is denoted by $t_{i,2}$.

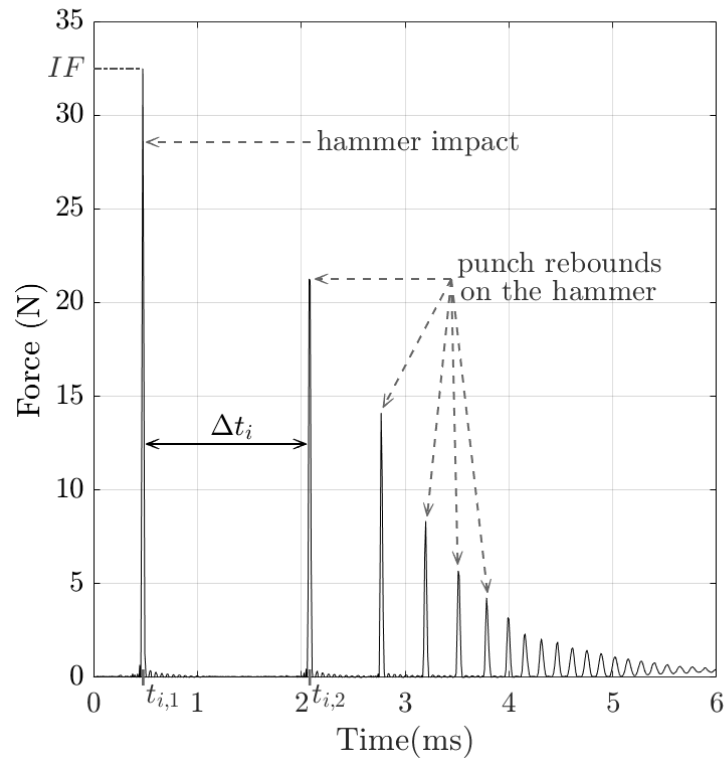


Figure 2: Example of a signal recorded by the force sensor impacting the hammer (impact #i) with a 3% agar-based phantom mimicking soft tissues. The temporal indicator $\Delta t_i = t_{i,1} - t_{i,2}$, where $t_{i,1}$ is the time of impact hammer and $t_{i,2}$ is the time of the first rebound of the punch on the hammer, and the impact force IF are indicated. Here, $\Delta t_i = 1.61$ ms and $IF = 32.5$ N.

A post-processing method adapted from Poudrel *et al.*^{15,22} was applied to signals with an IF comprised between 30 and 35 N, which will be discussed in section 4.2. The indicator $\Delta t_i = t_{i,2} - t_{i,1}$ was then determined for each impact #i.

Finally, the indicator Δt is defined by:

$$\Delta t = \frac{1}{5} \sum_{i=1}^5 \Delta t_i \quad (2)$$

which corresponds to the average value of five consecutive impacts. For each sample, five values of Δt were determined in order to assess the reproducibility of the measurements, which leads to a total of 25 impacts having an IF comprised between 30 N and 35 N. Eventually, the average and standard deviation values of all five measurements of Δt were determined for each sample.

2.3 MyotonPro

As shown in Fig. 3, MyotonPro (MyotonAS, Tallinn, Estonia) is a commercial handheld digital palpation device used for non-invasive characterization of soft tissues such as muscles, tendons, fascia or skin³³. We followed the measurement process prescribed by the manufacturer, which consists in positioning the device with the standard probe perpendicular to the sample. Then, the tool applied a pre-compression force of 0.18 N followed by a mechanical pulse of 0.4 N for 0.15 ms. The tissue response was recorded using an accelerometer. After post-processing of the acceleration, velocity and displacement signals, five parameters (the oscillation frequency, the dynamic stiffness, the logarithmic decrement, the mechanical stress relaxation time and the ratio of relaxation and deformation time) were estimated to define the viscoelastic properties of the soft tissue^{34,35}. In this study, only the dynamic stiffness S , defined by the manufacturer as the resistance of the tissues to a force of deformation produced by the mechanical pulse was recorded. S is given by³³:

$$S = \frac{a_{max} \times m_{probe}}{\Delta l} \quad (3)$$

where a_{max} is the vertical acceleration at the instant of maximum contact compression force and Δl is the displacement at the same instant and m_{probe} is the mass of the probe. For each sample, 15 measurements were realized with the test mode. The pulse time was equal to 0.07 ms¹³ to enable measurements of all mass concentration of agar-based phantoms. The average and standard deviation values of S were determined.

2.4 Dynamic mechanical analysis

A custom vibration-based set-up³⁶ was applied to 5 cylindrical samples (length: 80 mm and diameter: 40 mm) with agar mass concentrations of 1%, 2%, 3%, 4% and 5%, in order to assess their respective Young's modulus. The system consists of a mini shaker (type 4810, B&K, Naerum, Denmark) connected to an impedance head (type 8001, B&K, Naerum, Denmark), onto which is screwed a support for the agar sample. The measurement protocol consists in imposing a displacement with the shaker under the form of a chirp function between 20 and 800 Hz with a peak-to-peak amplitude equal to 0.015 mm. The system's responses in

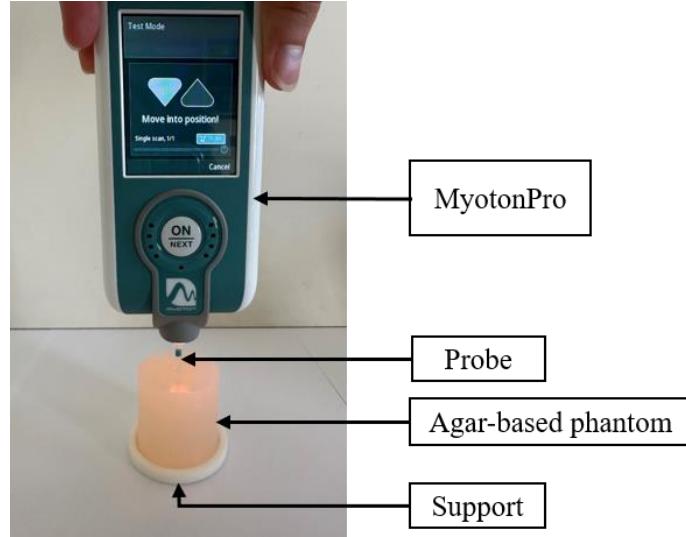


Figure 3: Experimental set-up using MyotonPro device to characterize a 3% agar-based phantom mimicking soft tissues.

force $F_M(t)$ and acceleration $\ddot{z}(t)$ were recorded in the z direction using the impedance head, as shown in Fig. 4.

As described in Ewins³⁷ and Silva *et al.*³⁸, the output of the impedance head had to be corrected, because the mass of the support could not be neglected compared to the mass of the sample. The force sensor of the impedance head records a force $F_M(t)$ which writes³⁷:

$$F_M(t) = F_T(t) + F_{app}(t) \quad (4)$$

where $F_T(t)$ is the force transmitted to the sample and $F_{app}(t)$ is the force applied to the support of the sample. The transfer functions $Y_M(f)$ and $Y_{corr}(f)$ are defined as:

$$Y_M(f) = \frac{\hat{z}(f)}{\hat{F}_M(f)} \text{ and } Y_{corr}(f) = \frac{\hat{z}(f)}{\hat{F}_T(f)}, \quad (5)$$

where $\hat{F}_M(f)$, $\hat{F}_T(f)$, $\hat{F}_{app}(f)$ and $\hat{z}(f)$ are the Fourier transforms of $F_M(t)$, $F_T(t)$, $F_{app}(t)$ and $\ddot{z}(t)$, respectively. The same custom vibration-based set-up is performed without any sample, which leads to the determination of $F_{M_{no-load}}(t)$ and $\ddot{z}_{no-load}(t)$, and to their respective Fourier transforms, $\hat{F}_{M_{no-load}}(f)$ and $\hat{z}_{no-load}(f)$. The spectral apparent mass $m_{app}(f)$ is then obtained following^{39,40}:

$$m_{app}(f) = \frac{\hat{F}_{M_{no-load}}(f)}{\hat{z}_{no-load}(f)} \quad (6)$$

$\hat{F}_{app}(f)$ can then be expressed as:

$$\hat{F}_{app}(f) = m_{app}(f) \times \hat{z}(f) \quad (7)$$

Following the correction method described in Cakar *et al.*³⁹ and Keswick *et al.*⁴⁰, it was possible to express the corrected transfer function Y_{corr} from the transfer function taken at the output of the impedance head, Y_M and the spectral apparent mass, m_{app} following :

$$Y_{corr}(f) = \frac{\hat{z}(f)}{\hat{F}_T(f)} = \frac{\hat{z}(f)}{\hat{F}_M(f) - m_{app}(f) \times \hat{z}(f)}$$

$$\Rightarrow Y_{corr}(f) = \frac{Y_M(f)}{1 - m_{app}(f) \times Y_M(f)} \quad (8)$$

By modeling the agar-based phantom as a linear elastic rod beam of length $L = 80 \text{ mm}$ and diameter $\varnothing = 40 \text{ mm}$, which is excited by an imposed displacement at its lower end (at $z = 0$) and is free upper face (at $z = L$), the Young's modulus of the phantoms E can be determined by⁴¹:

$$E = 4\rho(Lf_1)^2 \quad (9)$$

where f_1 is the fundamental resonance frequency of $Y_{corr}(f)$ and ρ is the density of the agar-based phantom.

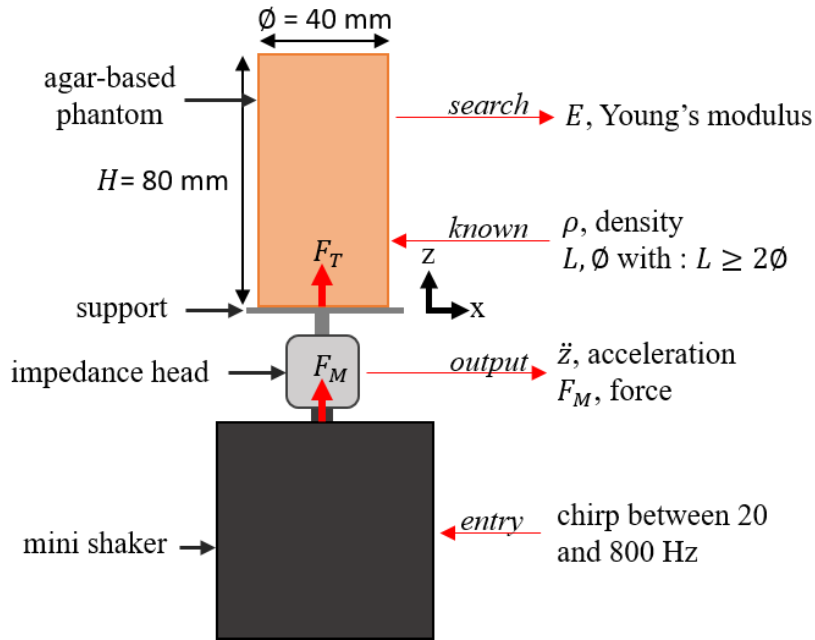


Figure 4: Schematic illustration of the custom vibration-based set-up performed on agar-based phantoms mimicking soft tissues to determine their Young's modulus.

2.5 Characterization protocols

Various phantoms were manufactured following the protocol described in subsection 2.1 in order to compare the performances of the IBAM and of MyotonPro. To do so, three series of experiments described hereafter were performed.

Estimation of the measured volume of interest (VOI). The aim of the first series of experiments was to determine the volume of interest (VOI) to which the method is sensitive for both measurement techniques. To do so, we considered cylindrical phantoms with 3% agar and varying diameter and length. First, several phantoms with a constant length of 40 mm and with diameters ranging from 10 to 60 mm were tested in order to determine the sensitivity of both techniques to the sample diameter. Second, another cylindrical phantom, with a diameter of 40 mm and a length of 50 mm was made. Both methods were first applied on this sample and then for successive decreasing lengths of the sample. To do so, the sample length was progressively reduced by a few millimeters using a cutting guide and the new length was re-evaluated using a digital caliper. This procedure was reproduced until the sample length was equal to 1.6 mm, so that the axial measuring range of both measurement methods could be assessed.

Axial and lateral resolution using bilayer configurations. For the second series of experiments, the purpose was to evaluate the axial and lateral resolutions of the two methods following the protocol schematically described in Fig. 5. To assess the axial resolution, two 80 mm long and 40 mm diameter cylindrical bilayer phantoms of 2% and 5% agar mass concentration were considered. For the first configuration, the bottom layer of the phantom was 40 mm long and made of hydrogel with 2% agar, while the top layer thickness $h_{5\%}$ (made of 5% agar) was varied between 0 and 40 mm with a step comprised between 2 and 6 mm, as shown in Fig. 5-A). This configuration will be referred to as “rigid on soft” in what follows. For the second configuration, the bottom layer of the phantom was 40 mm thick and made of hydrogel with 5% agar, while the top layer thickness $h_{2\%}$ (made of 2% agar) was varied between 0 and 40 mm with a step comprised between 2 and 6 mm, as shown in Fig. 5-A). This configuration will be referred to as “soft on rigid” in what follows.

To assess the lateral resolution, a bilayer phantom of 2% and 5% agar, consisting of two 40 mm cubes placed side by side, were considered, one for each measurement technique. From these phantoms, several series of measurements were performed by translating the two devices along the x -axis passing through the upper surface of the phantom, defined by the blue line in Fig. 5-B). A measurement was taken every 1 mm using the IBAM and every 2 mm using MyotonPro to avoid being affected by the previous measurement.

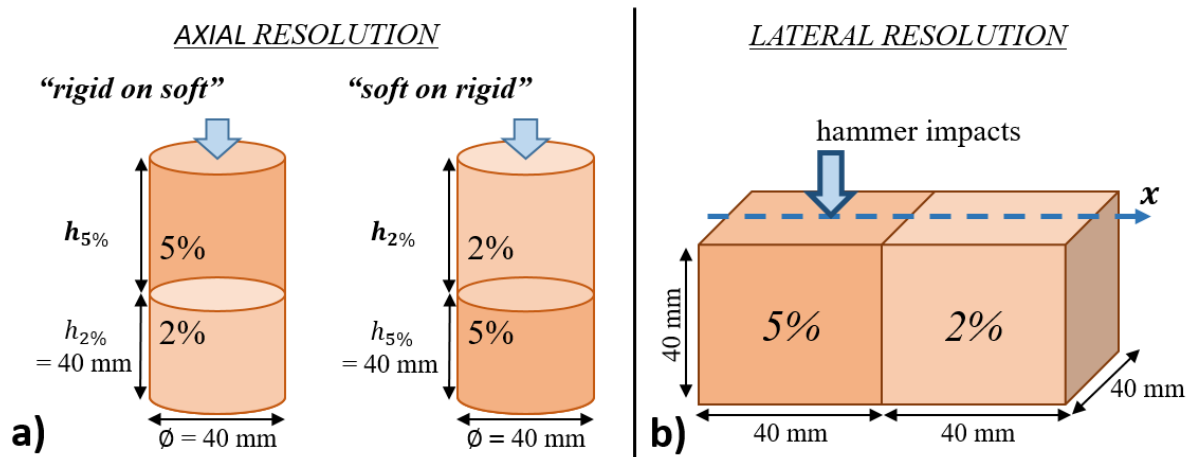


Figure 5: Illustration of the two experimental protocols for the estimation of the spatial resolution for IBAM and MyotonPro. **a)** Evaluation of the axial resolution for the two conditions “rigid on soft” and “soft on rigid” where the top layer thickness $h_{5\%}$ and $h_{2\%}$ (in bold on the figure) vary between 40 mm and 0 mm and **b)** evaluation of the lateral resolution.

Stiffness discrimination. The objective of the third series of experiments was to determine the effect of the agar mass concentrations, which is related to the stiffness, on the results obtained with both measurement techniques. To do so, five 40 mm long and 40 mm diameter cylindrical phantoms with agar mass concentrations of 1%, 2%, 3%, 4% and 5% were considered.

5

3. Results

3.1 Volume of interest (VOI) of the measurement

Figure 6 shows the variations of the indicators Δt and S obtained with the IBAM and MyotonPro as a function of the sample diameter for a constant length of 40 mm. The error bars correspond to the reproducibility of the measurements. The indicator Δt stays approximately constant for diameters larger than 15 mm, while the indicator S still varies until around 40 mm.

Figure 7 shows the variations of the indicators Δt and S obtained with the IBAM and MyotonPro as a function of the sample length for a constant diameter of 40 mm. The error bars correspond to the reproducibility of the measurements. The indicator Δt stays approximately constant for lengths larger than 5 mm, while the indicator S still varies until around 30 mm.

15

These two results indicate that the VOI of IBAM is smaller than that of Myoton, so that IBAM is less sensitive to the sample size compared to MyotonPro.

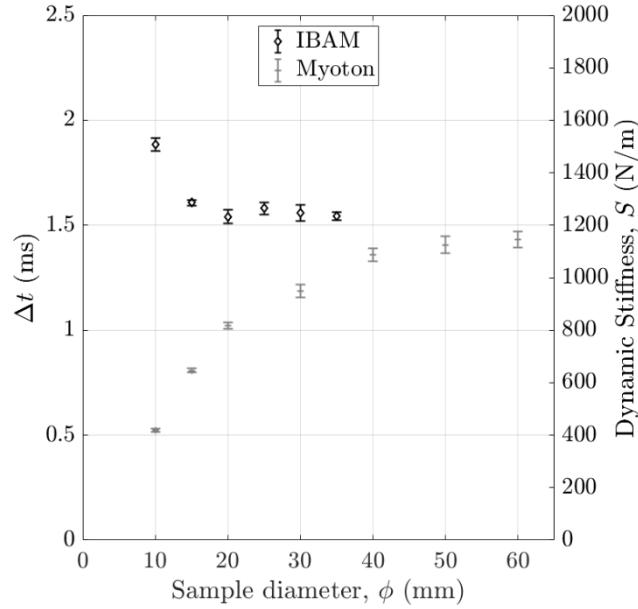


Figure 6: Variation of the indicators Δt and S obtained with the IBAM and MyotonPro as a function of the sample diameter with a 3% agar mass concentration. The error bars correspond to the reproducibility of the measurements.

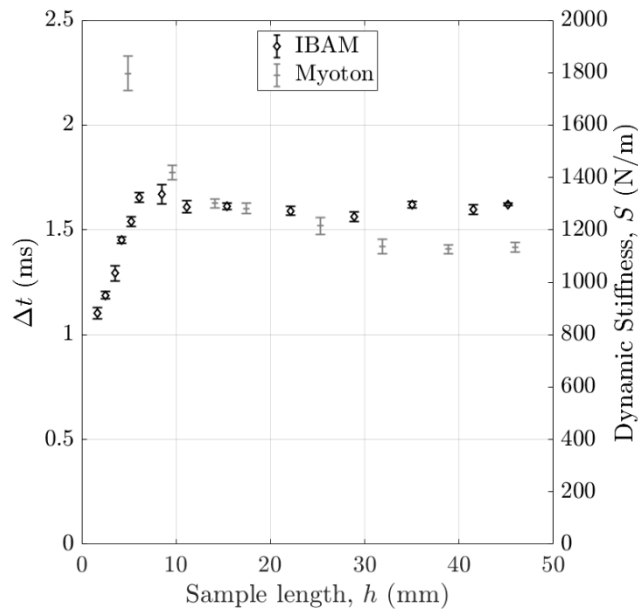


Figure 7: Variation of the indicators Δt and S obtained with the IBAM and MyotonPro as a function of the sample length with a 3% agar mass concentration. The error bars correspond to the reproducibility of the measurements.

3.2 Axial resolution

Figure 8 shows the variations of the indicators Δt and S obtained with the IBAM and MyotonPro as a function of $h_{5\%}$ for the “rigid on soft” configuration. The error bars correspond to the reproducibility of the measurements. The indicator Δt stays constant for values of $h_{5\%}$ larger than 10 mm, while the indicator S stays approximately constant for $h_{5\%}$ larger than 25

mm. Note that for both indicators, the values obtained for $h_{5\%}=0$ and for $h_{5\%}=40$ mm are similar the ones obtained with samples with mass concentration of 2% and 5%, respectively. In Fig. 8, the black dashed line (respectively the grey dash-dotted line) is the linear regression of Δt (respectively S) as a function of $h_{5\%}$, indicating the slope $a_5^{\Delta t}$ (respectively a_5^S) between $h_{5\%}=0$ mm and $h_{5\%}=8$ mm (respectively between $h_{5\%}=0$ mm and $h_{5\%}=20$ mm). For both methods, the values of slopes $a_5^{\Delta t}$ and a_5^S will be given and exploited in the subsection “Axial and lateral resolution” of the section 4.2 in the Discussion.

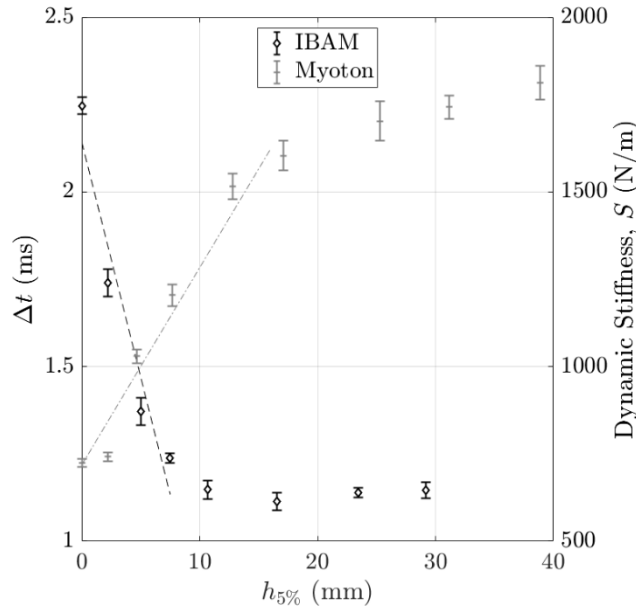


Figure 8: Variation of the indicators Δt and S obtained with the IBAM and MyotonPro as a function of the top layer thickness $h_{5\%}$ for the “rigid on soft” configuration. The error bars correspond to the reproducibility of the measurements.

Figure 9 shows the variations of the indicators Δt and S obtained with the IBAM and MyotonPro as a function of $h_{2\%}$ for the “soft on rigid” configuration. The error bars correspond to the reproducibility of the measurements. The indicator Δt remains constant for values of $h_{2\%}$ larger than 9 mm, while the indicator S remains constant for values of $h_{2\%}$ larger than 25 mm. Note that for both indicators, the values obtained for $h_{2\%}=0$ and for $h_{3\%}=30$ mm are similar to the ones obtained with samples with mass concentration of 5% and 2%, respectively. In the Fig. 9, the black dashed line (respectively the grey dash-dotted line) is the linear regression of Δt (respectively S) as a function of $h_{2\%}$, indicating the slope $a_2^{\Delta t}$ (respectively a_2^S) between $h_{5\%}=0$ mm and $h_{2\%}=8$ mm (respectively between $h_{5\%}=0$ mm and $h_{2\%}=15$ mm). For both methods, the values of slopes $a_2^{\Delta t}$ and a_2^S will be given and exploited in the subsection “Axial and lateral resolution” of the section 4.2 in the Discussion.

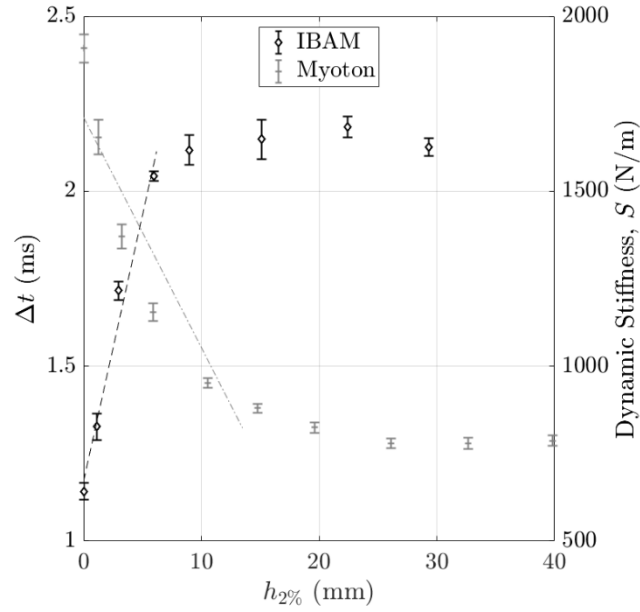


Figure 9: Variation of the indicators Δt and S obtained with the IBAM and MyotonPro as a function of the top layer thickness $h_{2\%}$ for the “soft on rigid” configuration. The error bars correspond to the reproducibility of the measurements.

3.3 Lateral resolution

Figure 10 shows the variations of the indicators Δt and S obtained with the IBAM and MyotonPro as a function of the position x of the device compared to the bilayer samples. The origin of the x -axis corresponds to the intersection between the two samples. The error bars correspond to the reproducibility of the measurements. The indicator Δt stays constant for values of x lower than -7 mm and larger than 2 mm, while the indicator S stays constant for values of x lower than -9 mm and larger than 15 mm. Note that the values obtained for both indicators for the minimal value of x and for the maximal value of x are similar the ones obtained with samples with mass concentration of 5% and 2% , respectively. In Fig. 10, the black dashed line (respectively the grey dash-dotted line) corresponds to the linear regression of Δt (respectively S) as a function of x , leading to an estimation of the slope $a_x^{\Delta t}$ (respectively a_x^S) between $x = -5$ mm and $x = 1$ mm (respectively between $x = -7$ mm and $x = 11$ mm). For both methods, the values of slopes $a_x^{\Delta t}$ and a_x^S will be given and exploited in the subsection “Axial and lateral resolution” of the section 4.2 in the Discussion.

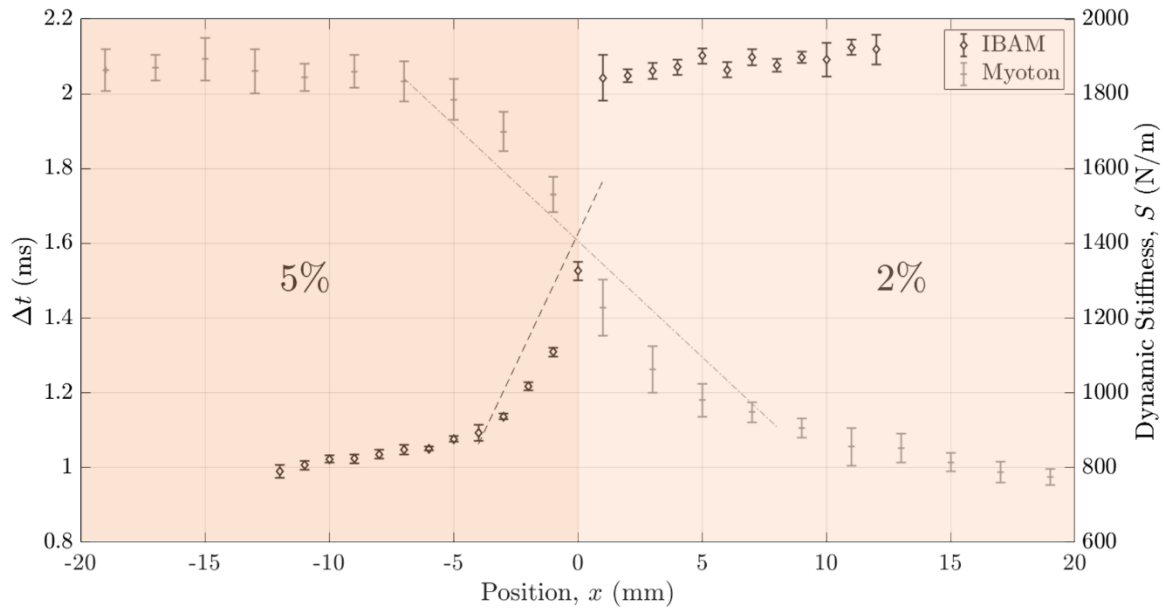


Figure 10: Variation of the indicators Δt and S obtained with the IBAM and MyotonPro as a function of the measurement position x on the upper surface of the bilayer samples. The error bars correspond to the reproducibility of the measurements. The color corresponds to the color indicated in Fig. 5.

3.4 Stiffness discrimination

Figure 11 shows the variations of the indicators Δt and S obtained with the IBAM and MyotonPro as a function of the sample Young's modulus measured with the custom vibration-based set-up described in Section 2.4 for agar mass concentration ranging from 1% to 5%. The error bars correspond to the reproducibility of the measurements. Both devices can discriminate between the five samples according to their stiffness. Δt (respectively S) is shown to decrease (respectively increase) as a function of the sample Young's modulus increases.

4. Discussion

The aim of this study was to demonstrate the performance of the impact-based analysis method (IBAM) to assess the stiffness of agar-based phantoms. Soft tissue phantoms were used to assess the performance of our method and compare it with those of an existing device, the MyotonPro¹³. The IBAM has the advantages of being non-invasive, real-time, quantitative, easy to use and inexpensive.

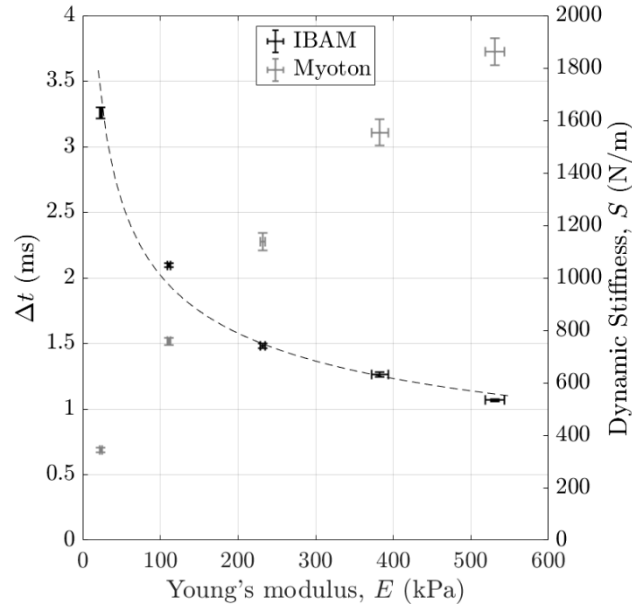


Figure 11: Variation of the indicators Δt and S obtained with the IBAM and MyotonPro as a function of the Young's modulus E of soft tissues phantoms obtained for agar mass concentrations varying between 1 and 5% using custom vibration-based set-up. The error bars correspond to the reproducibility of the measurements. The dashed line is the curve fitting with a power function of Δt as a function of E .

4.1 Young's modulus of agar-based phantoms mimicking soft tissues

The characteristics of agar hydrogels are very sensitive to preparation conditions and difficult to control^{30,31}. For example, the elastic properties of various agar gel with the same mass concentration have been shown to vary by one or even two orders of magnitude as a function of agar mass concentration³⁰. Figure 12 compares the variation of the sample Young's modulus as a function of the agar mass concentration found herein with previous results obtained in the literature using elastography with magnetic resonance imaging (MRE) or with optical coherence tomography (OCE), quasi-static compression test or DMA^{26,42-44}. Our results are shown to be consistent with other studies and to be acceptable to mimic healthy and abnormal soft tissue¹.

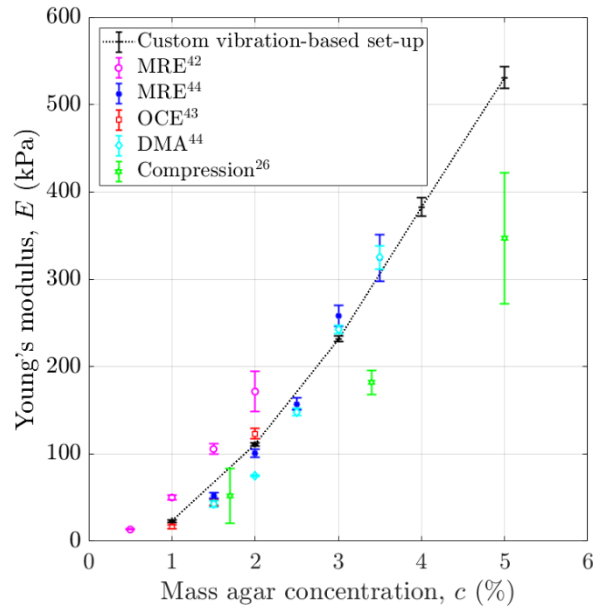


Figure 12: Comparison of the variation of the Young's modulus of soft tissues phantoms E as a function of the agar mass concentrations using various measurement methods. The error bars correspond to the reproducibility of the measurements.

4.2 Physical interpretation of Δt and S

Effect of the impact force. As shown in Poudrel *et al.*¹⁵, the average value of the indicator Δt as well as its reproducibility depend on the maximum value of the impact force IF . In order to optimize the reproducibility of the measurement, an impact was taken into account only when IF was comprised between 30 N and 35 N. As demonstrated in Poudrel *et al.*¹⁵, the values of Δt decrease as a function of the impact force IF and tend to stabilize above 30 N, which explains the lower bound of the interval. Moreover, the value of IF had to be minimized to avoid damaging the samples, which explains the upper bound. The range of variation of IF (5 N) was chosen sufficiently large to be able to reproduce the impact manually but not too large to minimize the variability.

Effect of the sample Young's modulus. As shown in Fig. 11, Δt decreases as a function of the Young's modulus, which is consistent with the results found in Poudrel *et al.*¹⁵. This decreasing behavior has been explained qualitatively by the fact that Δt may be inversely related to the resonance frequency of the punch and phantom system, as shown in the context of other applications of the methods like osteotomies^{22,25} or hip implant stability assessment¹⁸⁻²¹. Note that this behavior has been explained quantitatively using a 1D analytical model in Poudrel *et al.*¹⁵. Assuming that the hammer, the punch and agar-based phantom set-up can be modeled as a spring-mass system, the resonance frequency of the system can be simply modeled

as being proportional to the square root of the Young's modulus E of the agar-based phantom. Since Δt is inversely proportional to this resonance frequency, this assumption leads to:

$$\Delta t \propto E^{-0.5} \quad (10)$$

5 A logarithmic regression analysis of the data shown in Fig. 11 and represented with the dashed line indicates that:

$$\Delta t \propto E^{-0.36} \quad (11)$$

Despite the simplicity of the model which does not consider the geometry of the set-up nor the sample viscoelastic and nonlinear behavior, a good qualitative agreement is obtained with the experimental results.

10 The dynamic stiffness parameter S increases as a function the sample Young's modulus, which is also consistent with results realized with tissues mimicking phantoms⁴⁵ and biological soft tissues^{46,47}.

Effect of the volume of interest (VOI). The results shown in Figs. 6 and 7 indicate that the IBAM is not sensitive to changes of boundary conditions when located at a distance higher than
15 7,5 mm radially and 5 mm axially from the contact between the punch and the sample. These results indicate that for an agar mass concentration of 3%, the volume of interest (VOI) measured using the IBAM could be approximated by a hemi-sphere of radius approximately equal to 5 mm and centered on the center of the disc corresponding to the contact between the punch and the sample. However, these results may vary according to the agar mass
20 concentration as well as on the diameter of the punch. Following a simple dimensional analysis, the hemi-sphere radius should be determined by the diameter of the punch since no other dimension intervene in the system. The VOI measured using MyotonPro may be approximated by a hemi-sphere with a diameter around 30 mm, which indicates the lower VOI investigated by IBAM (5 mm, see above). Note that another probe may be used with MyotonPro (arm L-
25 shape probe, MyotonAS, Tallinn, Estonia) to allow superficial assessment of soft tissue⁴⁸ but this probe leads to an estimation of shear tissues properties⁴⁹.

Axial and lateral resolution. In the case of bilayer phantoms, Δt and S are sensitive to both layers when the measurement is performed close to their interface. Determining the errors on the estimation of the distance between the position of the center of the punch and the interface
30 may lead to a quantitative comparison of the axial and lateral resolutions of the IBAM and MyotonPro. To do so, for the "rigid on soft" configuration, a linear regression analysis,

represented by the dashed line in Fig. 8 was performed for Δt (respectively S) by considering the interval where Δt (respectively S) varies, so for $h_{5\%}$ lower than 10 mm (respectively $h_{5\%}$ lower than 25 mm) (see Fig. 8). The slope of the linear regression analysis obtained for Δt and S as a function of $h_{5\%}$ is noted $a_5^{\Delta t}$ and a_5^S , respectively. Moreover, the average reproducibility of both measurement techniques were determined by averaging the standard deviation values obtained in the same intervals for Δt and S and were noted $Err_5^{\Delta t}$ and Err_5^S . Following what has been done in Vayron *et al.*^{50,51}, the error on the estimation of $h_{5\%}$ using both measurements methods reads:

$$\varepsilon_5^{\Delta t} = \left| \frac{Err_5^{\Delta t}}{a_5^{\Delta t}} \right| \text{ (mm), for the IBAM} \quad (12)$$

$$\varepsilon_5^S = \left| \frac{Err_5^S}{a_5^S} \right| \text{ (mm), for MyotonPro} \quad (13)$$

The same method was applied to the results about the “rigid on soft” configuration shown in Fig. 9. We determined the slope of the linear regression analysis obtained for Δt and S as a function of $h_{2\%}$, noted $a_2^{\Delta t}$ and a_2^S by considering a linear regression analysis for both indicators Δt and S for $h_{2\%}$ lower than 9 mm and $h_{2\%}$ lower than 25 mm (see the dashed line in Fig. 9), which led to the determination of the error on the estimation of $h_{5\%}$ noted $\varepsilon_2^{\Delta t}$ and ε_2^S , respectively.

The same method was again applied to the results about the lateral resolution shown in Fig. 10 concerning the lateral resolution. We determined the slope of the linear regression analysis obtained for Δt and S as a function of x , noted $a_x^{\Delta t}$ and a_x^S by considering a linear regression analysis for both indicators Δt and S for x between -7 mm and 2 mm and respectively for x between -9 mm and 15 mm, (see the dashed line in Fig. 10), which led to the determination of the error on the estimation of x noted $\varepsilon_x^{\Delta t}$ and ε_x^S , respectively.

Table 1 shows the results obtained for the values of the reproducibility, the slope and the estimation error for the three aforementioned configurations and for the IBAM and MyotonPro. The values of the estimation error of $h_{5\%}$, $h_{2\%}$ and x obtained with the IBAM are shown to be significantly lower than the values obtained with MyotonPro. The results indicate the better sensitivity of the IBAM compared to MyotonPro. These results could be a step forward in the development of a future decision support system to delimit margins in the case of resection of diseased tissue with different mechanical properties.

Interface distance estimation error (mm)		Axial resolution		Lateral resolution
		"rigid on soft"	"soft on rigid"	
Method		$h_{5\%}$	$h_{2\%}$	x
Δt , Impact-based analysis method (IBAM)	$a^{\Delta t}$ (ms/mm)	-0.13	0.15	0.14
	$Err^{\Delta t}$ (ms)	0.03	0.03	0.02
	$\varepsilon^{\Delta t}$ (mm)	0.22	0.17	0.15
S , MyotonPro	a^S (N/m×mm)	56.51	-65.77	-62.17
	Err^S (N/m)	25.33	29.39	49.21
	ε^S (mm)	0.45	0.45	0.79

Table 1: Results of the interface distance estimation error, for the axial and lateral resolutions, with the IBAM and MyotonPro. a denotes to the slope of the linear fit of the result, Err denotes the average reproducibility and ε indicates the sensitivity of the measurements.

- 5 **Stiffness sensitivity comparison.** Following the same approach for the estimation error as the one described above, we also compared the performances of the IBAM with those of i) the custom vibration-based set-up and ii) MyotonPro to assess the sample stiffness by analyzing the results shown in Fig. 11, which is a simple way of determining the sensitivity of each method to changes of Agar mass concentration.
- 10 Because of the non-linear behavior of Δt and S as a function of the agar mass concentration, two ranges of variations were considered: i) between 1% and 2% and ii) between 1% and 5%. To do so, a linear regression analysis was performed with the data shown in Fig. 11 for both indicators Δt and S and both ranges of variation, respectively.

The slope of the linear regression analysis obtained for Δt and S are noted $a_E^{\Delta t}$ and a_E^S , respectively. Moreover, the average reproducibilities of both measurement techniques were determined by averaging all standard deviation values obtained in the corresponding range of variation and noted $Err_E^{\Delta t}$ and Err_E^S . Following what has been done in Vayron *et al*^{50,51}, the error on the estimation of the E using both measurements methods reads :

$$\varepsilon_E^{\Delta t} = \left| \frac{Err_E^{\Delta t}}{a_E^{\Delta t}} \right|, \text{ for the IBAM} \quad (14)$$

$$\varepsilon_E^S = \left| \frac{Err_E^S}{a_E^S} \right|, \text{ for MyotonPro} \quad (15)$$

The same method was applied to the results obtained with the custom vibration-based set-up using our samples and with literature data obtained with elastography and DMA for other agar-based phantoms^{26,42-44} (see Fig. 12). This analysis led to the determination of the error on the estimation of E using the aforementioned methods. Due to scarce data obtained in the literature^{26,42-44}, we could not consider both intervals for each dataset.

Experimental data		<i>agar mass concentration</i>	$a_E^{\Delta t}$ <i>ms/kPa</i>	$Err_E^{\Delta t}$ <i>ms</i>	$\varepsilon_E^{\Delta t}$ <i>kPa</i>
Δt , Impact-based analysis method (IBAM)		1% to 2%	-0.013	0.03	2.22
		1% to 5%	-0.003	0.02	5.42
			a_E^S <i>N/m × kPa</i>	Err_E^S <i>N/m</i>	ε_E^S <i>kPa</i>
S , MyotonPro		1% to 2%	4.73	10.86	2.29
		1% to 5%	2.94	31.28	10.65
			a_E^{DMA} <i>-</i>	Err_E^{DMA} <i>kPa</i>	ε_E^{DMA} <i>kPa</i>
Custom vibration-based set-up		1% to 2%	1	1.70	1.70
		1% to 5%	1	5.97	5.97
Literature data		<i>agar mass concentration</i>	a_E^{Lit} <i>-</i>	Err_E^{Lit} <i>kPa</i>	ε_E^{Lit} <i>kPa</i>
Elastography	DMA ⁴⁴	1% to 5%	1	5.30	5.30
	MRE ⁴⁴	1% to 5%	0.95	10.74	11.27
	MRE ⁴²	1% to 2%	0.92	7.98	8.71
	OCE ⁴³	1% to 2%	0.78	3.86	4.94

Table 2: Performances of different mechanical characterization methods (IBAM, MyotonPro, custom vibration-based set set-up, DMA, elastography with magnetic resonance imaging (MRE) and with optical coherence tomography (OCE)) assessed with samples with different agar mass concentrations. a denotes to the slope of the linear fit of the result as a function of the Young's modulus, Err denotes the average reproducibility and ε indicates the sensitivity of the measurements.

As shown in Table 2, the lowest error on the estimation of the sample stiffness in the range 1-2% is obtained using the custom vibration-based set-up, while this error (similar results are obtained herein and in the literature⁴⁴) is similar to the error using the IBAM when considering the entire concentration range (1-5%). However, custom vibration-based set-up and DMA are

difficult to be applied *in vivo*. Meanwhile, the IBAM has similar sensitivity than MyotonPro in the range 1-2%, but has a significantly better sensitivity i) compared to MyotonPro in the range 1-5% and ii) compared to all other techniques. Note that the IBAM is much simpler and cheaper compared to elastography.

5 4.3 Limitations and perspectives

First, we choose to use MyotonPro as the only device to establish a benchmark for comparison with the IBAM because it was shown to be the most effective for surface mechanical characterization of soft tissue⁵². However, in the future, the IBAM could also be compared with other surface stiffness measurement tools such as the Shore Durometer® (Type 10 1600-OO, Rex Gauge, Brampton, ON, Canada)^{13,52,53} or the IndentoPro® (Fascia Research Group, Ulm University; Department of Human Movement Sciences, University of Chemnitz, Germany)^{52,54}. Note that we did not use the Cutometer (Courage and Khazaka, Köln, Germany)^{6,7,12} because after preliminary tests, no measurement could be performed using our 5 agar-based phantoms.

15 Second, the reproducibility of hammer impacts on the punch could be improved, for example, in terms of punch guidance or hammer motion, thanks to a possible automation of the impact. Moreover, even if the duration of the measurement with agar-based phantoms lasted less than 10 minutes, new samples that are more stable over time, more durable and with 20 standardized mechanical properties could be used to improve the methodology and reproducibility of the measurements. Nevertheless, only a quasi-static Young modulus without dissipative effects was taken into account in the mechanical characterization of the phantoms and the viscoelastic effects of agar-based samples^{26,31} was neglected.

Third, numerical modelling of the IBAM based on the model developed in Poudrel *et al.*¹⁵ or using finite element model could allow to study in more details the determinant of Δt 25 and to investigate the presence of other potential information, such as viscosity or non-linear geometrical/material effects.

5. Conclusion

This study investigates the performance of an impact-based analysis method (IBAM) to 30 assess the biomechanical properties of phantoms mimicking soft tissues, which is compared with the results obtained with MyotonPro. A temporal indicator Δt is derived from the force signal resulting from the impact between the instrumented hammer and a punch in contact with

the sample. Different homogeneous and bilayer agar-based samples were used to assess the spatial (axial and lateral) resolution together with the sensitivity to changes of Young's modulus of the IBAM and of MyotonPro. The performances of the two aforementioned techniques were compared with those of DMA and elastography (MRE and OCE). The IBAM was shown to have a volume of interest (VOI) affecting the results equivalent to a hemi-sphere of diameter approximately twice the diameter of the punch, lower than that of MyotonPro. Moreover, the IBAM is shown to be more sensitive to stiffness variation than MyotonPro or elastography and to be equivalent to DMA. The IBAM has the advantage of being easy-to-use, cheap, real-time, objective and non-invasive. This study paves the way for the development of a decision support system for diagnosis, the quantitative monitoring and evaluation of skin treatments for clinicians. A perspective could consist in a preclinical study in animals in order to demonstrate its applicability *in vivo*.

6. Funding

This project has received funding from the European Research Council (ERC) under Horizon 2020 (grant agreement #101147066, project ERC Proof of Concept AssesSkin), from the Agence Nationale de la Recherche (ANR) under the project OrthAncil (ANR-21-CE19-0035-03) and the project OrthoMat (ANR-21-CE17-0004). The authors acknowledge the support from CNRS Innovation for the Prematuration project CarImpact.

7. Authors' Contributions

A.B., AS.P., CH.FL., JP.M. and G.H. participated in the conceptualization of the study. A.B., AS.P., G.R., VH.N. and G.H. established the methodology. A.B. and C.B. performed the data acquisition. A.B., AS.P., C.B., G.R., VH.N. and G.H. analyzed the data. A.B. and G.H. wrote the paper. G.R., CH.FL., JP.M and G.H. obtained the funding. G.H. was in charge of project administration. All authors have read and approved the final manuscript.

8. Declaration of Conflicting Interests

The authors declare that they have no financial or non-financial interests that are directly or indirectly related to the work submitted for publication.

9. Ethical Statement

This study did not require any ethical approval, as no human nor animal subjects were involved.

References

1. Krouskop TA, Wheeler TM, Kallel F, Garra BS, Hall T. Elastic moduli of breast and prostate tissues under compression. *Ultrason Imaging*. 1998;20(4):260-274. doi:10.1177/016173469802000403
2. Shiina T, Nightingale KR, Palmeri ML, et al. WFUMB Guidelines and Recommendations for Clinical Use of Ultrasound Elastography: Part 1: Basic Principles and Terminology. *Ultrasound Med Biol*. 2015;41(5):1126-1147. doi:10.1016/j.ultrasmedbio.2015.03.009
3. Skovoroda AR, Klishko A, Gusakyan DA, et al. Quantitative analysis of the mechanical characteristics of pathologically changed soft biological tissues. *Biophysics*. 1995;40:1359-1364.
4. Dobrev HP. In vivo study of skin mechanical properties in patients with systemic sclerosis. *J Am Acad Dermatol*. 1999;40(3):436-442. doi:10.1016/s0190-9622(99)70494-9
5. Gennisson JL, Baldeweck T, Tanter M, et al. Assessment of elastic parameters of human skin using dynamic elastography. *IEEE transactions on ultrasonics, ferroelectrics, and frequency control*. 2004;51(8):980-989. doi:10.1109/tuffc.2004.1324402
6. Dobrev H. Application of Cutometer area parameters for the study of human skin fatigue. *Skin Res Technol*. 2005;11(2):120-122. doi:10.1111/j.1600-0846.2005.00090.x
7. Stroumza N, Bosc R, Hersant B, Hermeziu O, Meningaud JP. Intérêt du cutomètre pour l'évaluation de l'efficacité des traitements cutanés en chirurgie plastique et maxillo-faciale. *Revue de Stomatologie, de Chirurgie Maxillo-faciale et de Chirurgie Orale*. 2015;116(2):77-81. doi:10.1016/j.revsto.2015.02.002
8. Ud-Din S, Bayat A. Non-invasive objective devices for monitoring the inflammatory, proliferative and remodelling phases of cutaneous wound healing and skin scarring. *Exp Dermatol.ge*. 2016;25(8):579-585. doi:10.1111/exd.13027
9. Gennisson JL, Deffieux T, Fink M, Tanter M. Ultrasound elastography: principles and techniques. *Diagn Interv Imaging*. 2013;94(5):487-495. doi:10.1016/j.diii.2013.01.022
10. Catheline S, Gennisson JL, Fink M. Measurement of elastic nonlinearity of soft solid with transient elastography. *J Acoust Soc Am*. 2003;114(6):3087-3091. doi:10.1121/1.1610457
11. Sandrin L, Fourquet B, Hasquenoph JM, et al. Transient elastography: a new noninvasive method for assessment of hepatic fibrosis. *Ultrasound Med Biol*. 2003;29(12):1705-1713. doi:10.1016/j.ultrasmedbio.2003.07.001
12. Ryu HS, Joo YH, Kim SO, Park KC, Youn SW. Influence of age and regional differences on skin elasticity as measured by the Cutometer. *Skin Res Technol*. 2008;14(3):354-358. doi:10.1111/j.1600-0846.2008.00302.x
13. Dellalana LE, Chen F, Vain A, et al. Reproducibility of the durometer and myoton devices for skin stiffness measurement in healthy subjects. *Skin Res Technol*. 2019;25(3):289-293. doi:10.1111/srt.12646
14. Lee Y, Kim M, Lee H. The Measurement of Stiffness for Major Muscles with Shear Wave Elastography and Myoton: A Quantitative Analysis Study. *Diagnostics (Basel)*. 2021;11(3):524. doi:10.3390/diagnostics11030524

15. Poudrel AS, Bouffandeau A, Demeet OL, Rosi G, Nguyen VH, Haiat G. Characterization of the concentration of agar-based soft tissue mimicking phantoms by impact analysis. *J Mech Behav Biomed Mater.* 2024;152:106465. doi:10.1016/j.jmbbm.2024.106465
- 5 16. Michel A, Bosc R, Vayron R, Haiat G. In vitro evaluation of the acetabular cup primary stability by impact analysis. *J Biomech Eng.* 2015;137(3). doi:10.1115/1.4029505
17. Michel A, Bosc R, Meningaud JP, Hernigou P, Haiat G. Assessing the Acetabular Cup Implant Primary Stability by Impact Analyses: A Cadaveric Study. *PLoS One.* 2016;11(11):e0166778. doi:10.1371/journal.pone.0166778
- 10 18. Michel A, Nguyen VH, Bosc R, et al. Finite element model of the impaction of a press-fitted acetabular cup. *Med Biol Eng Comput.* 2017;55(5):781-791. doi:10.1007/s11517-016-1545-2
19. Albin Lomami H, Damour C, Rosi G, et al. Ex vivo estimation of cementless femoral stem stability using an instrumented hammer. *Clin Biomech (Bristol, Avon).* 2020;76:105006. doi:10.1016/j.clinbiomech.2020.105006
- 15 20. Dubory A, Rosi G, Tijou A, Lomami HA, Flouzat-Lachaniette CH, Haiat G. A cadaveric validation of a method based on impact analysis to monitor the femoral stem insertion. *J Mech Behav Biomed Mater.* 2020;103:103535. doi:10.1016/j.jmbbm.2019.103535
21. Tijou A, Rosi G, Vayron R, et al. Monitoring cementless femoral stem insertion by impact analyses: An in vitro study. *J Mech Behav Biomed Mater.* 2018;88:102-108. doi:10.1016/j.jmbbm.2018.08.009
- 20 22. Hubert A, Rosi G, Bosc R, Haiat G. Using an Impact Hammer to Estimate Elastic Modulus and Thickness of a Sample During an Osteotomy. *J Biomech Eng.* 2020;142(7):071009. doi:10.1115/1.4046200
- 25 23. Bas Dit Nuges M, Rosi G, Hériveaux Y, Haiat G. Using an Instrumented Hammer to Predict the Rupture of Bone Samples Subject to an Osteotomy. *Sensors (Basel).* 2023;23(4):2304. doi:10.3390/s23042304
24. Lamassoure L, Giunta J, Rosi G, et al. Anatomical subject validation of an instrumented hammer using machine learning for the classification of osteotomy fracture in rhinoplasty. *Med Eng Phys.* 2021;95:111-116. doi:10.1016/j.medengphy.2021.08.004
- 30 25. Lamassoure L, Giunta J, Rosi G, Poudrel AS, Bosc R, Haiat G. Using an impact hammer to perform biomechanical measurements during osteotomies: Study of an animal model. *Proc Inst Mech Eng H.* 2021;235(7):838-845. doi:10.1177/09544119211011824
26. Manickam K, Machireddy RR, Seshadri S. Characterization of biomechanical properties of agar based tissue mimicking phantoms for ultrasound stiffness imaging techniques. *J Mech Behav Biomed Mater.* 2014;35:132-143. doi:10.1016/j.jmbbm.2014.03.017
- 35 27. Manickam K, Machireddy RR, Seshadri S. Study of ultrasound stiffness imaging methods using tissue mimicking phantoms. *Ultrasonics.* 2014;54(2):621-631. doi:10.1016/j.ultras.2013.08.018
28. Ismail HM, Pretty CG, Signal MK, Haggars M, Zhou C, Chase JG. Mechanical behaviour of tissue mimicking breast phantom materials. *Biomed Phys Eng Express.* 2017;3(4):045010. doi:10.1088/2057-1976/aa7992

29. Hall TJ, Bilgen M, Insana MF, Krouskop TA. Phantom materials for elastography. *IEEE Transactions on Ultrasonics, Ferroelectrics, and Frequency Control*. 1997;44(6):1355-1365. doi:10.1109/58.656639
- 5 30. Oyen ML. Mechanical characterisation of hydrogel materials. *International Materials Reviews*. 2014;59(1):44-59. doi:10.1179/1743280413Y.0000000022
31. Nayar VT, Weiland JD, Nelson CS, Hodge AM. Elastic and viscoelastic characterization of agar. *J Mech Behav Biomed Mater*. 2012;7:60-68. doi:10.1016/j.jmbbm.2011.05.027
32. Ebenstein DM, Pruitt LA. Nanoindentation of soft hydrated materials for application to vascular tissues. *J Biomed Mater Res A*. 2004;69(2):222-232. doi:10.1002/jbm.a.20096
- 10 33. Bizzini M, Mannion AF. Reliability of a new, hand-held device for assessing skeletal muscle stiffness. *Clin Biomech (Bristol, Avon)*. 2003;18(5):459-461. doi:10.1016/s0268-0033(03)00042-1
34. John AJUK, Galdo FD, Gush R, Worsley PR. An evaluation of mechanical and biophysical skin parameters at different body locations. *Skin Res Technol*. 2023;29(2):e13292. doi:10.1111/srt.13292
- 15 35. Myoton AS. MyotonPro Digital Palpation Device USER MANUAL. Published online November 30, 2022. www.myoton.com
36. Menard KPM Noah. *Dynamic Mechanical Analysis*. 3rd ed. CRC Press; 2020. doi:10.1201/9780429190308
37. Ewins DJ. *Modal Testing: Theory, Practice and Application*. Wiley; 2000.
- 20 38. Silva JMM, Maia NMM, Ribeiro AMR. CANCELLATION OF MASS-LOADING EFFECTS OF TRANSDUCERS AND EVALUATION OF UNMEASURED FREQUENCY RESPONSE FUNCTIONS. *Journal of Sound and Vibration*. 2000;236(5):761-779. doi:10.1006/jsvi.1999.2993
- 25 39. Cakar O, Sanliturk KY. Elimination of transducer mass loading effects from frequency response functions. *Mechanical Systems and Signal Processing*. 2005;19(1):87-104. doi:10.1016/S0888-3270(03)00086-4
40. Keswick PR, Norton MP. A comparison of modal density measurement techniques. *Applied Acoustics*. 1987;20(2):137-153. doi:10.1016/0003-682X(87)90059-4
41. Rao SS. *Vibration of Continuous Systems*. John Wiley & Sons; 2019.
- 30 42. Hamhaber U, Grieshaber FA, Nagel JH, Klose U. Comparison of quantitative shear wave MR-elastography with mechanical compression tests. *Magn Reson Med*. 2003;49(1):71-77. doi:10.1002/mrm.10343
43. Han Z, Li J, Singh M, et al. Quantitative methods for reconstructing tissue biomechanical properties in optical coherence elastography: a comparison study. *Phys Med Biol*. 2015;60(9):3531-3547. doi:10.1088/0031-9155/60/9/3531
- 35 44. Ringleb SI, Chen Q, Lake DS, Manduca A, Ehman RL, An KN. Quantitative shear wave magnetic resonance elastography: comparison to a dynamic shear material test. *Magn Reson Med*. 2005;53(5):1197-1201. doi:10.1002/mrm.20449

45. Dougherty J, Schaefer E, Nair K, Kelly J, Masi A. Repeatability, Reproducibility, and Calibration of the MyotonPro® on Tissue Mimicking Phantoms. In: American Society of Mechanical Engineers Digital Collection; 2014. doi:10.1115/SBC2013-14622
- 5 46. Kelly JP, Koppenhaver SL, Michener LA, Proulx L, Bisagni F, Cleland JA. Characterization of tissue stiffness of the infraspinatus, erector spinae, and gastrocnemius muscle using ultrasound shear wave elastography and superficial mechanical deformation. *J Electromyogr Kinesiol.* 2018;38:73-80. doi:10.1016/j.jelekin.2017.11.001
47. Feng YN, Li YP, Liu CL, Zhang ZJ. Assessing the elastic properties of skeletal muscle and tendon using shearwave ultrasound elastography and MyotonPRO. *Sci Rep.* 2018;8(1):17064. doi:10.1038/s41598-018-34719-7
- 10 48. Rosicka K, Mierzejewska-Krzyżowska B, Mrówczyński W. Comparison of different MyotonPRO probes for skin stiffness evaluation in young women. *Skin Res Technol.* 2021;27(3):332-339. doi:10.1111/srt.12946
49. Junker HJ, Thumm B, Halvachizadeh S, Mazza E. A quantitative comparison of devices for in vivo biomechanical characterization of human skin. *Mech Soft Mater.* 2023;5(1):5. doi:10.1007/s42558-023-00053-w
- 15 50. Vayron R, Mathieu V, Michel A, Haiat G. Assessment of in vitro dental implant primary stability using an ultrasonic method. *Ultrasound Med Biol.* 2014;40(12):2885-2894. doi:10.1016/j.ultrasmedbio.2014.03.035
- 20 51. Vayron R, Nguyen VH, Lecuelle B, Haiat G. Evaluation of dental implant stability in bone phantoms: Comparison between a quantitative ultrasound technique and resonance frequency analysis. *Clin Implant Dent Relat Res.* 2018;20(4):470-478. doi:10.1111/cid.12622
52. Bartsch K, Brandl A, Weber P, et al. Assessing reliability and validity of different stiffness measurement tools on a multi-layered phantom tissue model. *Sci Rep.* 2023;13(1):815. doi:10.1038/s41598-023-27742-w
- 25 53. Kissin EY, Schiller AM, Gelbard RB, et al. Durometry for the assessment of skin disease in systemic sclerosis. *Arthritis Rheum.* 2006;55(4):603-609. doi:10.1002/art.22093
54. Koch V, Wilke J. Reliability of a New Indentometer Device for Measuring Myofascial Tissue Stiffness. *J Clin Med.* 2022;11(17):5194. doi:10.3390/jcm11175194